Can. J. Remote Sensing, Vol. 30, No. 5, pp. 840–853, 2004

An assessment of the VIC-3L hydrological model for the Yangtze River basin based on remote sensing: a case study of the Baohe River basin

Suoquan Zhou, Xu Liang, Jing Chen, and Peng Gong

Abstract. As a first step in our effort to simulate terrestrial hydrological processes for the entire Yangtze River basin, a hydrologically based three-layer variable infiltration capacity (VIC-3L) land surface model is applied to the Baohe River basin, which has a drainage area of 2500 km^2. Water fluxes of the Baohe River basin are simulated using the VIC-3L model at a spatial resolution of approximately 4 km. The soil and land cover properties were taken from the resource and environment database (scale 1 : 4 000 000) of China (REDC). The vegetation and land cover data were also derived from the moderate resolution imaging spectroradiometer (MODIS) data over the study area. Measurements from a number of weather stations were used to obtain meteorological forcings for each modeling grid based on a stepwise interpolation approach (SIA). The VIC-3L model was run at a daily time step. Differences in model-simulated water fluxes resulting from using the two different data sources (i.e., MODIS versus REDC) on information of land cover classification and leaf area index (LAI) were compared. Model-simulated daily runoff was routed through the Baohe River basin network and compared with the daily observed streamflow measured at Jiangkou hydrological station at the outlet of the Baohe River basin from 1992 to 2001. Results from the VIC-3L model simulations using REDC data compare well with the observations in general, but the model-simulated streamflows often underestimate the observed peak flows significantly. In comparison, the underestimations of the peak flows are significantly improved when more accurate vegetation information on land cover and LAI from MODIS is used. The REDC land cover was obtained about 20 years ago with only six different types of vegetation that are generally distributed homogeneously throughout the study region. However, the land cover in the Baohe River basin is mainly mixed forest. The unrealistically large land cover area of deciduous broadleaf forest in the REDC data source resulted in an unreasonable increase in evapotranspiration and a decrease in streamflows. This study indicates clearly the important role that remote sensing (e.g., MODIS data) plays in improving model simulations.

Résumé. À titre de première étape dans notre travail de simulation des processus hydrologiques terrestres pour l'ensemble du bassin du fleuve Yangtsé, nous avons appliqué un modèle hydrologique de surface à capacité d'infiltration variable à trois couches distribué spatialement (VIC-3L) au bassin du fleuve Baohe, couvrant une zone de drainage de 2500 km^2. Les flux d'eau du bassin du fleuve Baohe sont simulés à l'aide du modèle VIC-3L à une résolution spatiale d'environ 4 km. Les propriétés du sol et du couvert ont été dérivées de la base de données sur les ressources et l'environnement (échelle 1 : 4 000 000) de la Chine (REDC) tandis que les données sur la végétation et le couvert ont été dérivées des données MODIS (« moderate-resolution imaging spectroradiometer ») de la région. Des mesures provenant d'un certain nombre de stations météorologiques ont aussi été utilisées pour obtenir un forçage météorologique pour chacun des points de la grille de modélisation basé sur une méthode d'interpolation par étape (SIA). On a fait tourner le modèle VIC-3L à un pas d'une journée. On a comparé les différences dans les flux d'eau simulés par le modèle suite à l'utilisation de ces deux sources de données (i.e., MODIS versus REDC) au niveau de l'information sur la classification du couvert et de l'indice de surface foliaire (LAI). Les débits journaliers simulés par le modèle ont été distribués à travers le réseau du bassin du fleuve Baohe et comparés aux débits journaliers observés à la station hydrologique de Jinagkou, à la sortie du bassin du fleuve Baohe, de 1992 à 2001. Les résultats des simulations du modèle VIC-3L utilisant les données REDC concordent bien en général avec les observations quoique les débits simulés par le modèle sous-estiment souvent de façon significative les débits de pointe observés. En comparaison, les sous-estimations de débit maximal sont significativement améliorées lorsque l'on utilise l'information plus précise relative à la végétation dérivée des données de couvert et de LAI de MODIS. Les données du couvert dérivées de la base REDC ont été obtenues il y a environ 20 ans et ne comportaient que six types différents de végétation répartis de façon homogène à travers la zone d'étude. Or, le couvert du bassin du Baohe est principalement composé de forêt mixte. La surface anormalement élevée de forêt de feuillus observée dans la base de données REDC a

Received 15 October 2003. Accepted 1 April 2004.

S. Zhou.[1] Nanjing Institute of Meteorology, Key Laboratory of Meteorological Calamity, Nanjing 210044, Jiangsu, China.

X. Liang. Department of Civil and Environmental Engineering, University of California, Berkeley, CA 94720-1710, USA.

J. Chen and P. Gong. International Institute for Earth System Science, Nanjing University, Nanjing 210093, China.

[1]Corresponding author (e-mail: zhousuoquan@jsmail.com.cn).

entraîné une augmentation démesurée de l'évapotranspiration et une réduction dans les débits. Cette étude montre de façon évidente le rôle important que la télédétection (i.e. les données MODIS) peut jouer dans l'amélioration des simulations de modèles.
[Traduit par la Rédaction]

Introduction

Applications of remote sensing in hydrological studies and water resources management can be categorized as follows: (*i*) using original remote sensing imagery directly to identify hydrologically important spatial phenomena; (*ii*) using processed remote sensing data, such as precipitation, as forcings of hydrological models; (*iii*) using multispectral data, such as vegetation (land cover) types and density, to quantify surface parameters; (*iv*) direct calculation of evapotranspiration distribution in terms of spectral data of satellite remote sensing based on surface energy balance (e.g., Bastiaanssen et al., 1998); (*v*) using remote sensing derived fields, such as soil moisture, to improve model simulations through data assimilations; and (*vi*) validating model simulations using remote sensing data. Accurate model simulations depend on a number of factors, such as good parameterizations of physical processes, a balanced representation of model complexity, good model input forcings, and good model parameters. Remotely sensed data can, at least, improve model simulations by (*i*) providing more accurate spatially distributed model parameters such as vegetation information over a study region, and (*ii*) helping to identify potential model structure weaknesses through validation, data assimilation, etc.

Accurate estimation of the spatial distribution of actual evapotranspiration over a large region is very challenging, but critically important for land surface models to obtain reasonable partitions of water and energy fluxes in water and energy budgets. Although good progress has been made towards estimating the spatial distribution of evapotranspiration based on remotely sensed data (e.g., Bastiaanssen et al., 1998; Jiang and Islam, 2001; Ayenew, 2003), most of them are not yet at a satisfactory level. Errors in the approximation of surface energy balance components lead to errors in evapotranspiration estimations. As pointed out by Gillies et al. (1997), estimation of the evapotranspiration distribution with satellite remote sensing remains a challenge. Therefore, a promising approach to obtaining reasonable estimation of the spatial distribution of evapotranspiration at present is to estimate the evapotranspiration by land surface models with an effective use of remote sensing information. For instance, vegetation parameters, such as land cover and leaf area index (LAI), are important factors for obtaining accurate evapotranspiration estimation. Current remote sensing techniques have the capability of providing relatively reliable information on land cover type and LAI (e.g., Engman, 1996; Ritchie and Rango, 1996; Kim and Barros, 2002). Therefore, incorporating such new remote sensing information (e.g., new spatial vegetation information with high resolution to allow multiple land cover types to coexist within a model computational grid cell) into land surface models may lead to significant improvement in evapotranspiration estimations, which would then lead to improvement in calculations of other components in the land surface models.

Although the potential of remote sensing has been widely recognized, there are few examples of successful applications in hydrological simulations (Engman, 1996; Ritchie and Rango, 1996). It is still difficult to select and interpret appropriate spectral data and extract useful information for hydrological process studies. Among remotely sensed information, hydrologically significant variables that are underutilized are vegetation parameters derived from optical remote sensing. In particular, vegetation structural parameters, such as LAI and canopy closure, are important in precipitation interception and evapotranspiration and thus play a crucial role in land surface models.

The three-layer variable infiltration capacity (VIC-3L) model (Liang et al., 1994; 1996a; 1996b; 1999; 2003; Cherkauer and Lettenmaier, 1999; Liang and Xie, 2001) is a hydrologically based land surface scheme. Spatial variabilities of infiltration, precipitation, and vegetation are considered partially in the model to simulate water and energy budgets at the land surface. The dynamics of runoff generation includes two components, fast runoff and slow runoff. Direct runoff, including both saturation and infiltration excess runoff (Liang et al., 1994; Liang and Xie, 2001), represents the fast component, and the ARNO model subsurface flow (Francini and Pacciani, 1991; Todini, 1996) represents the slow component. The upper soil layer of the model is designed to represent the dynamic response of the soil to rainfall events, and the lower layer is used to characterize the seasonal soil moisture behavior through the slower dynamics of inter-storm period associated with deeper soil moisture and subsurface flow processes. In this application, we do not explicitly represent the groundwater table. In other words, the unsaturated and saturated zones are treated in a lumped sense. The VIC-3L model, however, can explicitly deal with the dynamics of surface and groundwater interactions and calculate the groundwater table (Liang et al., 2003). Besides the upper and lower layers, the VIC-3L model also has a thin topsoil layer, which allows for quick bare soil evaporation following small summer rainfall events. VIC-3L includes soil moisture diffusion processes between the three soil layers (Liang et al., 1996a) and can be applied in a cold climate where snow and frozen soil processes play important roles (Cherkauer and Lettenmaier, 1999). The model is driven by precipitation, maximum and minimum daily temperature (daily time step) or temperature for every sub-daily time step, and wind speed as an input for the full energy and water balance mode. Vegetation exerts important controls on the exchange of water and energy at the land surface and is therefore explicitly incorporated into

the model in a simple yet reasonable manner in which multiple land cover types (i.e., different vegetation cover and bare soil) and their corresponding LAIs are explicitly represented within each model grid and are prescribed–updated through input information. Specifically, the structure of the VIC-3L model allows, in principal, as many land cover types as possible within each model grid as long as such information is available.

The VIC-3L model and its variations (referred to as VIC) have been tested and applied to various basins of different scales with good performance (e.g., Nijssen et al., 1997; Wood et al., 1997; Liang and Xie, 2001; Parada et al., 2003). The VIC model has also performed well under humid and cold conditions in the various phases of the project for intercomparison of land surface parameterization schemes (PILPS) (e.g., Chen et al., 1997; Wood et al., 1998; Liang et al., 1998; Lohmann et al., 1998; Bowling et al., 2003; Nijssen et al., 2003). Liang and Xie (2001) and Parada et al. (2003) showed that the performance of the VIC-3L model under drier conditions could be improved with the inclusion of a new representation of the infiltration excess runoff mechanism. Furthermore, the VIC-3L model has been used in a wide range of applications, including soil moisture estimation (e.g., Nijssen et al., 2001a), streamflow forecasting (e.g., Nijssen et al., 2001b; Hamlet and Lettenmaier, 1999a; 1999b), and climate change impact analyses (e.g., Leung et al., 1999).

The VIC-3L model has been successfully applied to many regions in the world but not in the Yangtze River basin. The Yangtze River is the longest river in China, with a main channel length of 6300 km and a drainage area of 1 800 000 km^2. The Yangtze River basin includes large urban areas and significant croplands that play critical roles in the economy of China and the health of the ecological environment. There are many notable projects associated with the Yangtze River basin, such as the Three Gorges Dam project and the project involving the transfer of water from south to north in China. It is critical and at the same time challenging to understand the natural terrestrial hydrological processes over the Yangtze River basin and the interactions between land surface and atmosphere and the impact of the Three Gorges Dam on the surrounding ecological environment.

In this paper, the surface hydrological processes of a selected subbasin of the Yangtze River basin are simulated using the VIC-3L model with the conventional (i.e., resource and environment database of China (REDC)) and remote sensing surface vegetation coverage (i.e., moderate resolution imaging spectroradiometer (MODIS) data). The model simulations based on REDC data are compared with those based on MODIS data. Impacts of applying the remote sensing data on water fluxes are discussed. Simulation results are compared with 10-year daily streamflow measured at the outlet of the basin from 1992 to 2001.

Site description, data, and parameters

The Baohe River basin (**Figure 1**), bounded by latitudes 33°40′N to 34°20′N and longitudes 106°40′E to 107°30′E, is located in the upper Hanjiang River basin. Baohe basin has a drainage area of approximately 2500 km^2, covers Taibai, Fengxian, and Liuba counties, and has its outlet at Jiangkou hydrological station. Annual average precipitation ranges from 500 to 700 mm, and the terrain fluctuates from 1000 to 1200 m above sea level. The basin has good vegetation coverage, with 93%, 90%, and 50% coverage in Taibai, Fengxian, and Liuba counties, respectively. Vegetation cover includes oak, white poplar, oil pine, birch, walnut tree, sumach, and apple tree. The primary crops are corn, wheat, rice, and soybeans. The basin is close to natural protection regions for wildlife, such as giant salamander, giant panda, and ibis.

Daily precipitation, maximum temperature, minimum temperature, wind velocity, air pressure, vapor pressure, relative humidity, and sunshine hours are available for the period 1992–2001 from six meteorological stations. The locations of the six meteorological stations, Taibai, Baoji, Fengxian, Liuba, Chenggu, and Yangxian, are shown in **Figure 1b**. Daily climate variables required by the VIC-3L model were interpolated to 4 km resolution (for the

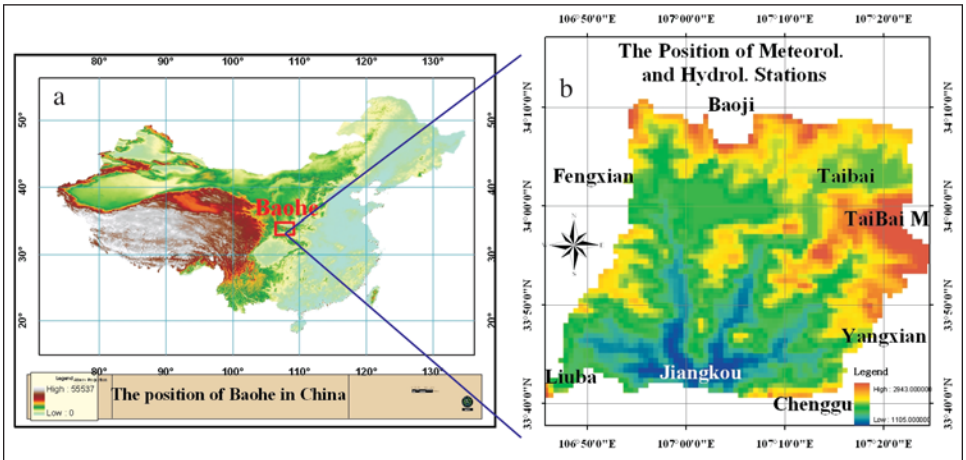

Figure 1. (a) Location of the Baohe River basin in China. (b) Locations of the meteorological and hydrological stations in the Baohe River basin.

interpolation method, see the section titled "Stepwise interpolation approach (SIA) for climate variables"). Daily observed streamflow time series at Jiangkou station (see **Figure 1b**) are also available from 1992 to 2001, except for 1994, 1997, and 1998.

Soil and vegetation data from the REDC

Spatial information on soil and vegetation for the Baohe River basin is available from the REDC data source (1 : 4 000 000) (see **Figure 2**). In the Baohe River basin the land cover classifications from the REDC include deciduous needleleaf forest, deciduous broadleaf forest, woody forest, open shrubland, grassland, and cropland. The vegetation types and their corresponding characteristics are listed in **Table 1**. The soil types from the REDC source include sandy loam, sandy clay loam, and clay loam. The soil types and their corresponding characteristics are listed in **Table 2**.

Soil and vegetation data from MODIS

The land cover and LAI data derived from the MODIS[2] data source were obtained from Boston University. The land cover is classified by a supervised International Geosphere–Biosphere Program (IGBP) classification technique. The images used were from the National Aeronautics and Space Administration (NASA) TERRA/MODIS HDF-EOS MOD12Q1. The IGBP classification scheme identifies 17 classes at 1 km resolution: (1) evergreen needleleaf forest, (2) evergreen broadleaf forest, (3) deciduous needleleaf forest, (4) deciduous broadleaf forest, (5) mixed forests, (6) closed shrublands, (7) open shrublands, (8) woody savannas, (9) savannas, (10) grasslands, (11) permanent wetlands, (12) croplands, (13) urban and built-up, (14) cropland – natural vegetation mosaic, (15) snow and ice, (16) barren or sparsely vegetated, and (17) water. Eight of these vegetation types are present in the Baohe River basin based on the MODIS data (see **Figure 3a**): deciduous needleleaf forest, deciduous broadleaf forest, mixed forests, woody forests, closed shrublands, open shrublands, grasslands, and croplands.

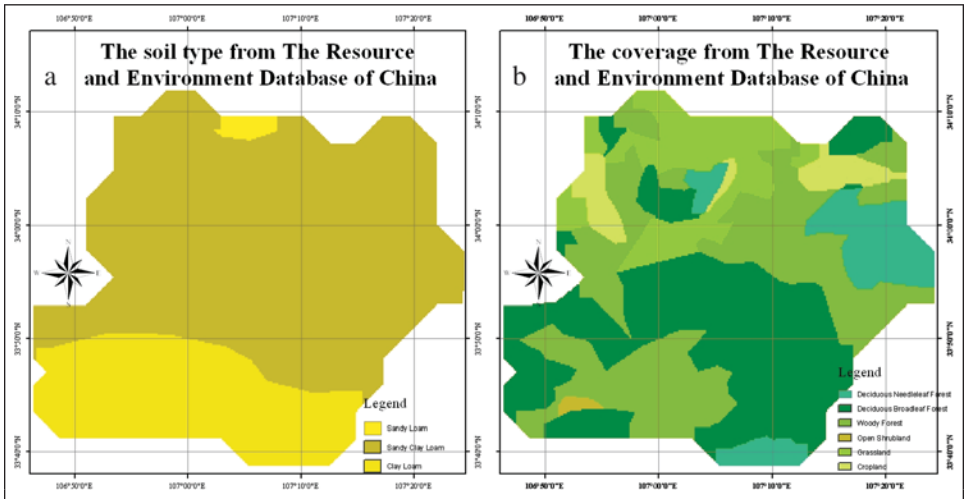

Figure 2. Spatial distributions of (a) soil type and (b) vegetation coverage in the Baohe River basin based on the resource and environment database of China (REDC).

Table 1. Vegetation types and their properties.

Class	Vegetation type	Overstory	r_{arc} (s/m)	r_{min} (s/m)	Albedo (m)	Roughness length (m)	Displ. (m)	R_{GL} (W/m^2)
3	Deciduous needleleaf forest	1	60	125	0.18	1.230	6.70	30
4	Deciduous broadleaf forest	1	60	125	0.18	1.230	6.70	30
5	Mixed cover	1	60	125	0.18	1.230	6.70	50
6	Woody forest	1	60	125	0.18	1.230	6.70	50
8	Closed shrubland	0	50	135	0.19	0.495	1.00	75
9	Open shrubland	0	50	135	0.19	0.495	1.00	75
10	Grassland	0	25	120	0.20	0.074	0.40	100
11	Cropland	0	25	120	0.20	0.012	0.33	100

Note: Displ., displacement; r_{arc}, architectural resistance of vegetation type; r_{min}, minimum stomatal resistance of vegetation type; R_{GL}, minimum incoming shortwave radiation at which there will be transpiration.

[2] MODIS data are available from ftp://crsa.bu.edu/pub/rmyneni/myneniproducts/MODIS/MOD15_BU/C4/LAI/data/1km/2000/ and http://duckwater.bu.edu/lc/mod12q1.html.

Table 2. Soil types and their properties.

USD class	Soil type	Sand (%)	Clay (%)	Bulk density (g/cm^3)	Field capacity (m^3/cm^3)	Wilting point (cm^3/cm^3)	Porosity fraction	Saturated hydraulic conductivity (cm/h)	Slope of retention curve, b
3	Sandy loam	69.28	12.48	1.57	0.21	0.09	0.40	5.24	4.84
7	Sandy clay loam	60.97	26.33	1.60	0.27	0.17	0.39	2.40	8.66
9	Clay loam	30.08	33.46	1.43	0.34	0.21	0.46	1.77	8.02

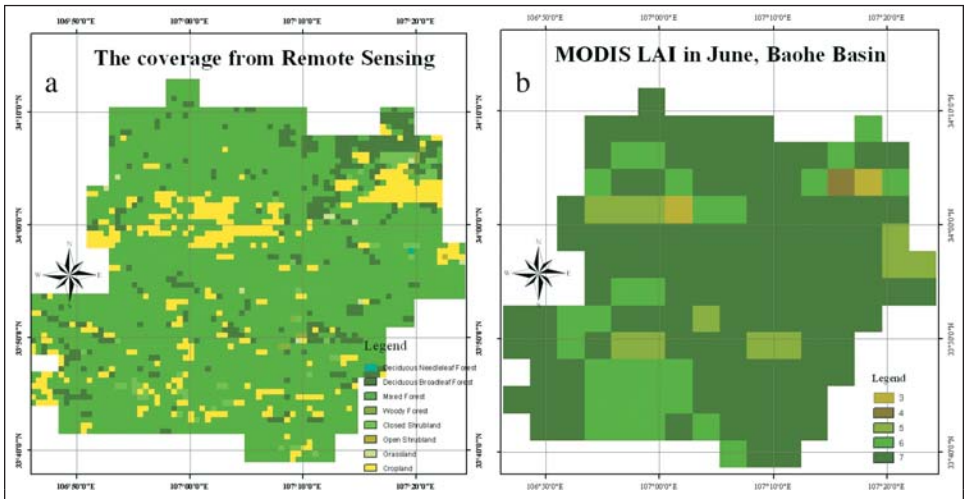

Figure 3. (a) Land cover classification for the Baohe River basin based on MODIS data for 2000 at 1 km resolution. (b) Spatial distribution of LAI in June 2000 for the Baohe River basin based on MODIS data at 4 km resolution.

The LAI information is available from the MOD15A2 product produced with the Knyazikhin algorithm (Knyazikhin et al., 1998a; 1998b) at 1 km resolution, which is aggregated to a spatial resolution of 4 km to be consistent with the spatial resolutions of other variables used in the VIC-3L model simulations. **Figure 3b** shows the spatial distributions of LAI for June 2000 at 4 km resolution for the Baohe River basin. **Figure 3** shows that the spatial distributions of LAI clearly vary greatly with seasons, and that there are large spatial variations of LAI in space. The temporal variation for croplands can be dramatic over the course of the life cycle (e.g., periods of planting, growing, and harvesting). Information with significant temporal and spatial variations in LAI is important for land surface models. Remote sensing is the ultimate source for timely information over a large spatial domain.

VIC-3L model parameters

In addition to the information on model input forcings (discussed in the next section), soil, and vegetation as discussed earlier (see **Tables 1** and **2**; and **Figures 2** and **3**), there are parameters that cannot be effectively determined or estimated based on the available soil and vegetation information. These parameters are called model parameters and generally need to be determined through a model calibration process. There are six such model parameters in the VIC-3L model: infiltration shape parameter b_i; soil depth of layers 2 (D_2) and 3 (D_3); and the three base flow related parameters D_m, D_s, and W_s, representing, respectively, the maximum subsurface flow, the fraction of D_m, and the fraction of maximum soil moisture in the third soil layer. The values used in this study for the six VIC-3L model parameters are shown in **Table 3** and are based on past experience of VIC-3L model applications.

Stepwise interpolation approach (SIA) for climate variables

Background information and introduction to the SIA

The climate variables, such as precipitation, temperature, and wind speed, are affected by terrain. Many researchers (e.g., Kurtzman and Kadmon, 1999; Oliver and Webster, 1990) have incorporated elevation into geostatistical approaches (Martínez-Cob, 1996; Prudhomme and Reed, 1999; Goovaerts, 2000). Others have developed methods to relate climate variables to various aspects of topography, such as altitude,

Table 3. Parameters of the VIC-3L model.

b_i	0.03
D_s	0.01
D_m (mm/h)	3.0
W_s	0.65
D_2 (m)	2.0
D_3 (m)	2.0

slope, aspect, and exposure, using regression equations (Basist et al., 1994; Goodale et al., 1998; Ninyerola et al., 2000; Wotling et al., 2000; Weisse and Bois, 2001). Marquínez et al. (2003) recently developed multiple linear regression relationships between precipitation and a range of topographic variables using a geographic information system. A typical interpolating error of the method was approximately 10%. There are limitations in the accuracy of using this method for mountain areas. Thus, Marquínez et al. established separate regression relationships to improve the interpolation accuracy for different areas.

In general, climate variables such as temperature and pressure are affected by the atmospheric circulation and thus have relatively homogeneous distributions in space. Affected by mesoscale and microscale convective systems, for instance, thunderstorms, lower jet stream, and tropical cyclones, precipitation has much more heterogeneous distributions in space and is closely related to terrain.

In this study, we use a stepwise interpolation approach (SIA) to obtain atmospheric forcings (i.e., precipitation, temperature, pressure, and wind) at finer spatial resolutions. SIA with Gauss distance weight can improve the accuracy (Zhou, 1993a; 1993b; 1995) at the grid cells by correcting computation errors step by step and incorporating topographic factors in the interpolation equations for precipitation, temperature, pressure, and wind. Specifically, the interpolation equations consider variations of elevation, slope, and aspect for precipitation, statistical lapse rate for temperature, logarithmic variation of elevation for wind speed, and pressure. Six meteorological stations shown in **Figure 1b** are used to establish the interpolating equations based on SIA to obtain the atmospheric forcings at 4 km resolution for the Baohe River basin.

SIA results for climate variables

Figure 4a shows a spatial distribution of 10-year (from 1992 to 2001) annual averaged temperature obtained with SIA at 4 km resolution. It can be seen that the temperature varies with topography. The average maximum annual temperature is 11.4 °C in the valley, and the average annual temperature generally decreases with an increase in elevation. The lowest temperature, 0.3 °C, is at the top of Taibai Mountain in the northeast of the basin. The spatial distribution of the interpolated temperature is consistent with the general spatial distribution of the observations for the region. **Figure 4b** shows a comparison of a 10-year daily averaged temperature between the observations and interpolated results at the Taibai County meteorological station in which the Taibai station was included in establishing the interpolation relationships owing to the limited number of available stations. The absolute errors are about 0.5–1.0 °C, and the relative errors are less than 5% from the interpolation equations.

Figure 4c shows the 10-year (from 1992 to 2001) averaged annual precipitation obtained from SIA. There is more precipitation in the south than in the north, and more in the valley than on the mountain tops. The analysis indicates that the precipitation decreases as elevation increases. **Figure 4d** shows the comparison between the 10-year averaged daily precipitation based on SIA and the observations at Taibai station, in which Taibai station was included to establish the interpolation equations, again owing to the limited number of available stations. The maximum error is about 8 mm in **Figure 4d**, and the relative error is approximately 10%.

Results with the REDC vegetation classification

The VIC-3L model is applied to the Baohe River basin at 4 km resolution. The atmospheric forcings required by the VIC-3L model are interpolated to the 4 km resolution based on SIA. Soil properties are used at the spatial resolution of the REDC data. Vegetation properties from the REDC data source are also used at the spatial resolution of the REDC data, and the vegetation information from the MODIS data source at 1 km resolution is aggregated to 4 km resolution. The main reason for selecting 4 km spatial resolution for this study is to keep a relative balance in obtaining a reasonable river network for the Baohe River basin, having reasonable spatial representation on vegetation heterogeneities, and avoiding significant deteriorations of the spatial distributions of the atmospheric forcings through the SIA method based on the limited available information. In this section, only the VIC-3L model simulation results using the REDC vegetation data are discussed.

Simulation of the components of surface water balance

Figures 5a–5d show spatial distributions of the annual mean evapotranspiration, total runoff, soil moisture of the top 10 cm layer, and snow sublimation obtained from the VIC-3L model simulations over the period 1992–2001 for the Baohe River basin. The soil and vegetation information used here (i.e., **Figure 5**) is from the REDC data source (see **Figure 2**). **Figure 5a** shows higher evapotranspiration in the southeast region and less in the northwest region. The spatial distribution of evapotranspiration is consistent with the general spatial patterns of precipitation (**Figure 5c**) and vegetation (**Figure 2b**). The maximum mean annual evapotranspiration of 588 mm/year occurs in the southern deciduous broadleaf forest area of Hanzhong District, which receives relatively more precipitation. The minimum averaged annual evapotranspiration, about 496 mm, occurs in the mountains with higher elevations and a dryer climate.

The spatial pattern of the simulated mean annual total runoff (**Figure 5b**) is different from that of evapotranspiration (**Figure 5a**). There is more runoff in the southeast basin that is related to the sufficient precipitation in the area and on Taibai Mountain in the northeast of the basin owing to steeper terrain and less evapotranspiration but greater snowmelt in the summer. Runoff is about 73 mm in the north and west of the basin because of lower precipitation. The cropland in the northeast of the basin has 231 mm of runoff, about 100 mm

more than in the rest of the basin. This is partially due to crop plantations and harvest.

Figure 5c shows the spatial distribution of the simulated mean annual soil moisture in the top 10 cm layer. The moisture in this thin layer of soil seems to be affected by the spatial distributions of both vegetation and precipitation. The soil moisture seems to be relatively homogeneous in the middle and southern parts of the basin. The heterogeneity of the soil moisture distribution seems to relate to the spatial distributions of vegetation, topography, soil properties, and precipitation in a complex manner, similar to the findings reported by other researchers (e.g., Famiglietti et al., 1999; Mohanty and Skaggs, 2001; Hupet and Vanclooster, 2002; Kim and Barros, 2002; Oldak et al., 2002). Furthermore, there seems to exist a soil moisture transition zone of roughly 4–8 km in length between two different soil types. The minimum mean annual soil moisture is less than 21 mm and occurred in the sandy loam area, and the maximum mean annual soil moisture is about 28 mm in the clay loam area. **Figure 5d** shows the spatial distribution of the snow sublimation. The southern part of the basin has a very low value of snow sublimation (approximately 2 mm), whereas the northern part of the basin over the mountain areas has high snow sublimation (e.g., approximately 27 mm).

The VIC-3L model simulated evapotranspiration at the model grid cell containing the meteorological station of Taibai County is compared with the potential evaporation measured at the station. A strict comparison between the two time series is not appropriate because of the differences in scales and the availability of water. That is, the VIC-3L model simulation at

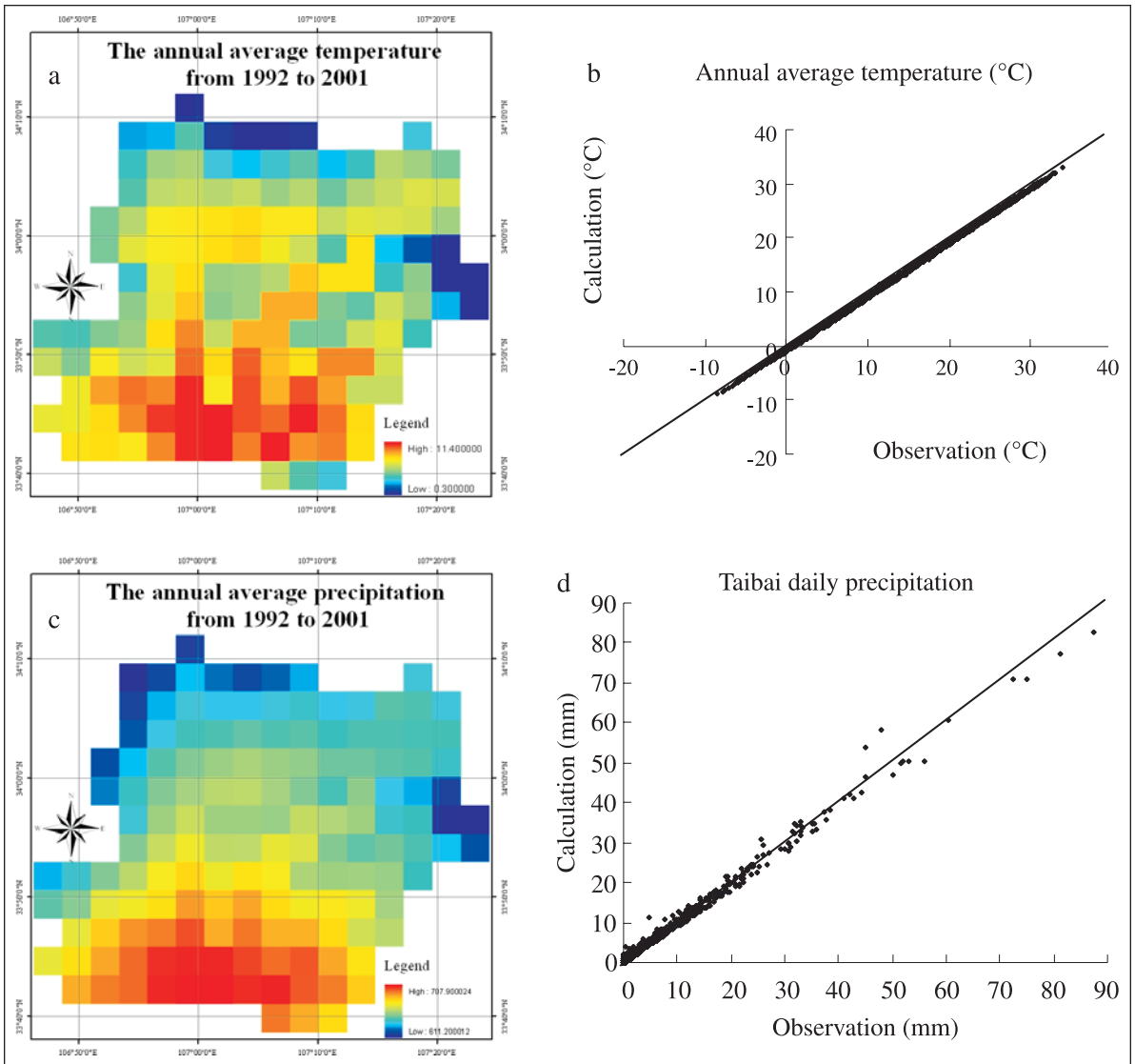

Figure 4. (a) Spatial distribution of 10-year (from 1992 to 2001) averaged annual temperature based on SIA. (b) Comparison between 10 year averaged daily temperature obtained from SIA and the observations measured at the Taibai meteorological station. (c) Spatial distribution of 10-year (from 1992 to 2001) averaged annual precipitation based on SIA. (d) Comparison between 10-year averaged daily precipitation obtained from SIA and the observations measured at the Taibai meteorological station.

the grid represents an average actual evapotranspiration over an area of 4 km × 4 km, not a potential evaporation at any point within the 4 km × 4 km grid area. A general comparison between the two time series is informative, however, in checking the general daily patterns simulated by the VIC-3L model. **Figure 6** shows a general comparison between the VIC-3L model simulated grid-averaged evapotranspiration and the observed point potential evaporation smoothed by a 15-day window for the period 1992–2001. It can be seen in **Figure 6** that the general pattern from the VIC-3L model compares well with the observations. As expected, the VIC-3L model simulated evapotranspiration is less than the observed point potential evaporation. The underestimation in the summer months is not as significant as expected, partially due to the vegetation classification based on the REDC data. The significant underestimation in the winter months by the VIC-3L model may be partially related to the vegetation information provided by the REDC data source and the dry climate in winter.

Simulation of river flow

Measured streamflow at the outlet of a watershed provides important information to partially test the performance of a model, since the streamflow is an integrated measure of the water over the watershed and can be measured with relatively high accuracy compared with the other water fluxes in the watershed. In our study, the river network at 4 km resolution is obtained based on the digital elevation model (DEM) at 1 km resolution using the method of Reed (2003) (see **Figure 7**). **Figure 7** shows that the river network obtained based on 4 km resolution is consistent with that based on 1 km resolution. To compare the VIC-3L model simulated runoff with the observed streamflow, the simulated runoff is routed through the river network using a simple routing model (Lohmann and Nolte-Holube, 1996).

Figure 8 compares the VIC-3L model daily routed runoff (broken lines) with the observed streamflow (solid lines) at the outlet of the Baohe River basin, Jiangkou hydrological station, for 5 years during the period 1992–2001. The VIC-3L model

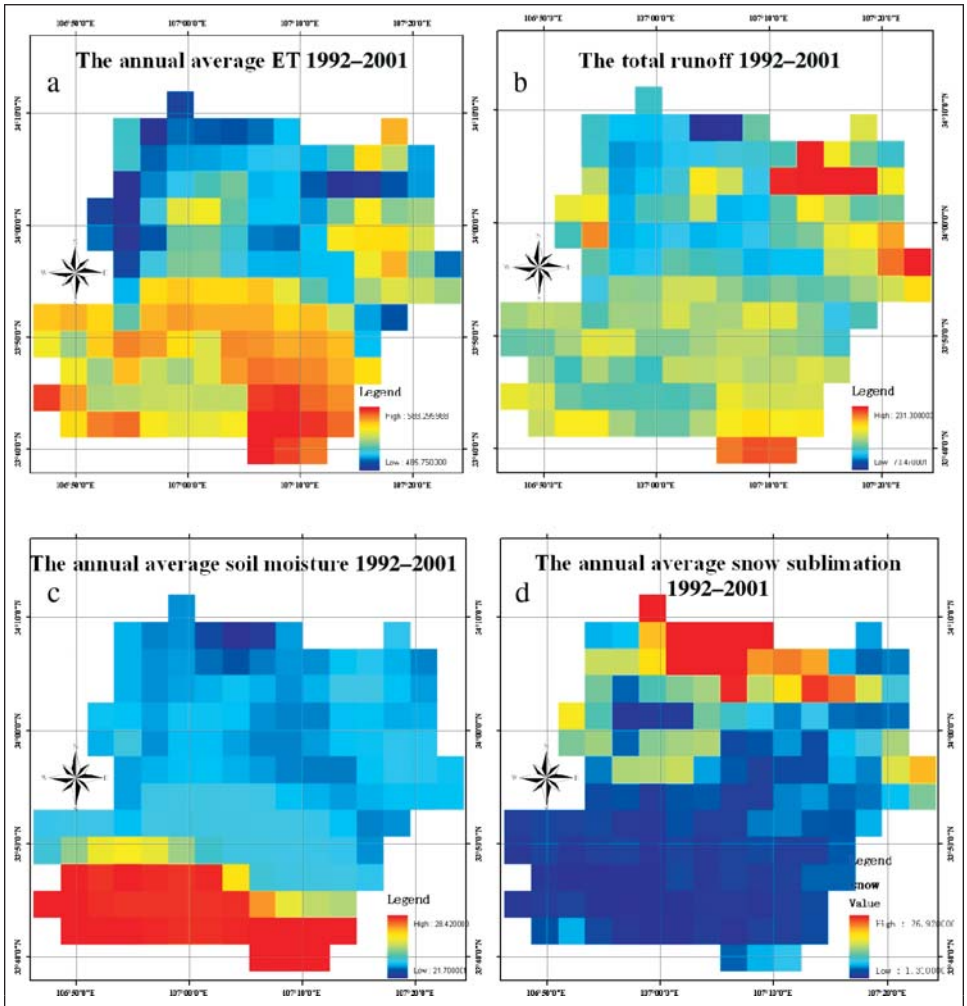

Figure 5. Spatial distributions (from 1992 to 2001) of the VIC-3L model simulation results using the REDC data source for vegetation for the Baohe River basin: (a) mean annual evapotranspiration, (b) mean annual runoff, (c) mean annual soil moisture in the top 10 cm layer, and (d) mean annual snow sublimation.

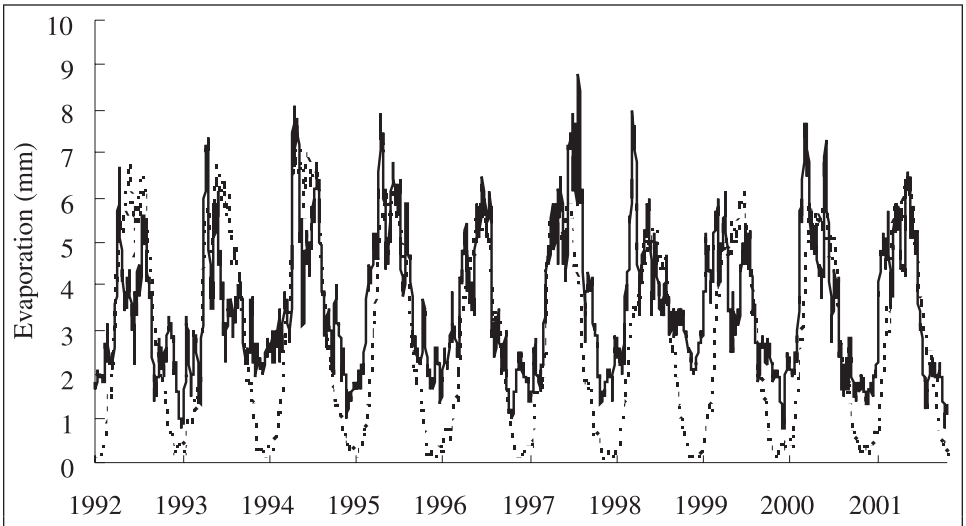

Figure 6. Daily time series of potential evaporation measured by evaporation pan (solid line) at the Taibai meteorological station and the VIC-3L model simulated evapotranspiration at the grid containing the observation station (broken line) for the period 1992–2001.

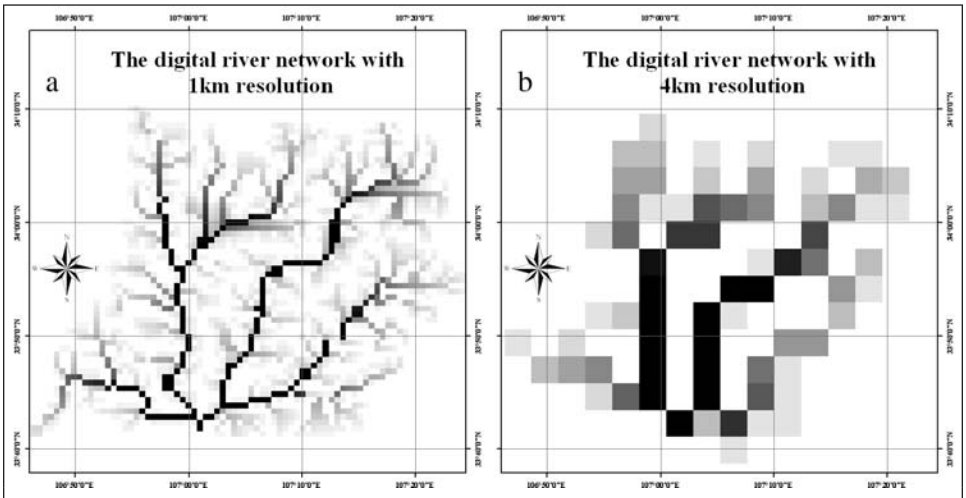

Figure 7. Digital river networks of the Baohe River basin based on (a) 1 km resolution DEM, and (b) 4 km resolution DEM.

simulated runoff compares well with the daily observed streamflow in general, but significant underestimations of the streamflow peaks are evident (see **Figure 8**). The underestimations may be affected by the inaccurate spatial distributions of vegetation, soil properties, and precipitation.

Impacts of remote sensing information on land surface modeling

To investigate the impacts of remote sensing on water fluxes simulated by the VIC-3L model for the Baohe River basin, we replaced the vegetation information from the REDC data source with the MODIS data while keeping everything else the same as described in previous sections. The VIC-3L model is rerun for the same period (i.e., 1992–2001) in which the MODIS vegetation information (i.e., LAI and vegetation classification) of year 2000 is applied to the 10-year simulation by assuming that vegetation did not change over the 10-year period in the study region. It is worth noting that it is desirable to have monthly land cover and LAI information each year to conduct the 10 year VIC-3L model simulations. However, such information is not available to this study. Although monthly land cover and LAI data were only available for 2000 from MODIS, the land use has not changed significantly in the study region over the past 10 years. Therefore, we use the monthly MODIS data for 2000 in the VIC-3L model simulations for the period 1992–2001.

Differences of surface fluxes in space

Figure 9 shows the differences in mean annual evapotranspiration, runoff, soil moisture in the top 10 cm layer, and snow sublimation fields between the VIC-3L model

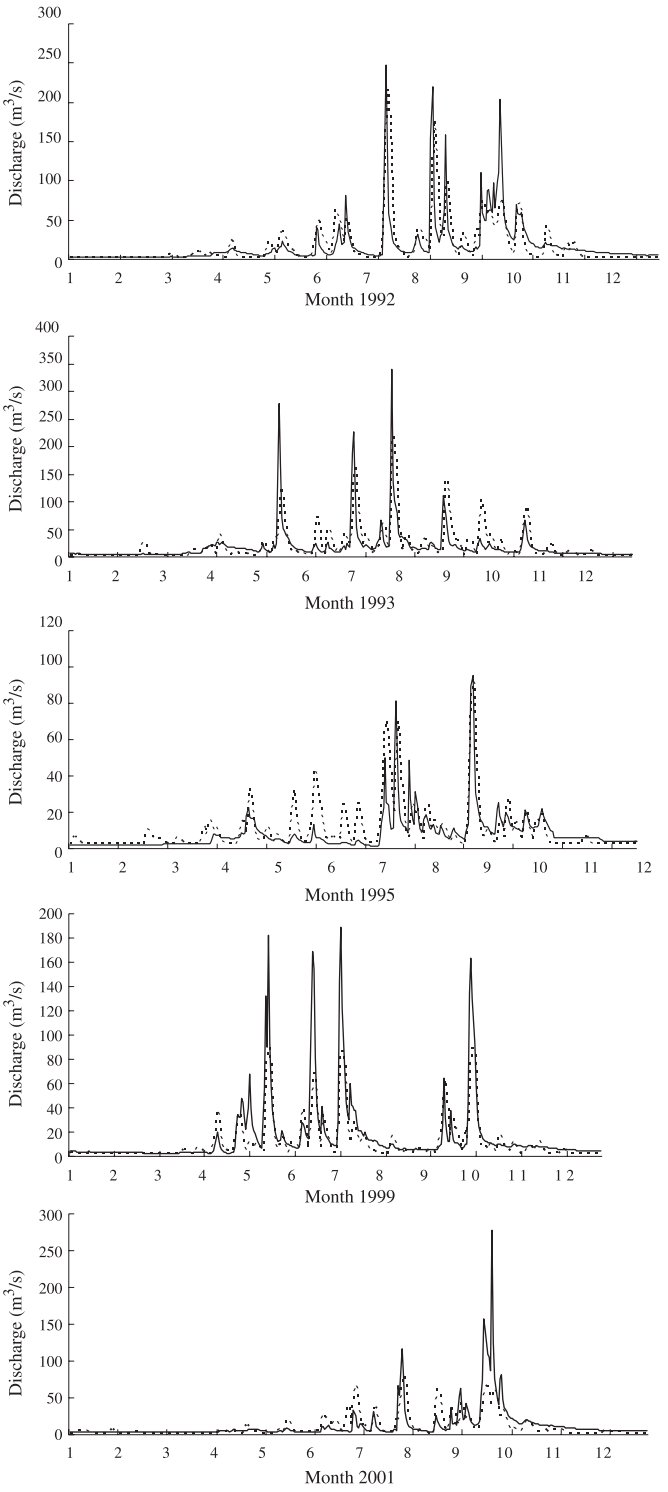

Figure 8. Comparison of the VIC-3L model simulated daily flow (broken lines) based on the REDC vegetation information with the observed streamflow (solid lines) at Jiangkou hydrological station at the outlet of the Baohe River basin for 5 years during the period 1992–2001.

simulations using MODIS data and those using REDC data. The relative differences in evapotranspiration (**Figure 9a**) vary from 10% to 18%, with the absolute differences ranging from –21 to +86 mm. In general, there is an increase in evapotranspiration in the northern part of the basin and a decrease in the southern part of the basin in the mean annual evapotranspiration measure. The increase in the north is mainly because of a different identification of vegetation cover by the MODIS data from that by the REDC data. In particular, the MODIS data indicate that the area is covered by cropland with high LAI values in the summer, whereas the REDC data indicate the area as grassland with low LAI values. The decrease in the south is also caused by the different identifications of the land cover from the MODIS and REDC data sources. Specifically, the MODIS data indicate that the area is covered by mixed forest, whereas the REDC data indicate the area is deciduous broadleaf forest. The overall impact of the MODIS vegetation data on the VIC-3L model simulation over the Baohe River basin is a reduction in evapotranspiration estimation.

Figure 9b shows the differences in mean annual runoff for the 10 years. The relative differences for runoff vary from 10% to 20%, similar in magnitude to those for evapotranspiration. The absolute differences in runoff range from 7 to 42 mm. The increases in runoff occur in the northern and southern parts of the Baohe River basin when the MODIS data are used, and the decreases occur in the middle part and the northeast mountain areas of the basin.

Figure 9c shows that the relative difference in the soil moisture in the top thin layer is less than 10%. With the use of MODIS data, the soil moisture is 1.6 mm less in the middle part of the basin and 8.0 mm more in the southern and northern parts of the basin when compared with the soil moisture obtained based on the REDC vegetation data. **Figure 9d** shows the difference in snow sublimation, which varies from 8 to 18 mm. The maximum positive difference is on the top of Taibai Mountain. This is reasonable because Taibai Mountain is covered with permanent snow.

Impact of MODIS data on the VIC-3L model runoff time series at Jiangkou hydrological station

Figure 10 shows the VIC-3L model runoff simulations at Jiangkou hydrological station using the MODIS vegetation information for the same 5 years as those shown in **Figure 8**. The solid line represents the observed streamflow, and the open circles represent the VIC-3L model simulated runoff. Compared with the VIC-3L model results shown in **Figure 8**, it can be seen that the MODIS vegetation information significantly improves the VIC-3L model runoff simulations for the Baohe River basin. In particular, the large underestimations of the streamflow peaks by the VIC-3L model shown in **Figure 8** are no longer present in **Figure 10**. In 1992, the improvement is obvious in September, with the VIC-3L model runoff peak close to the measured value. The MODIS data make the simulation peaks closer to the measured peaks in May, June, and July of 1993. In 1995, the VIC-3L model simulated runoff is closer to the observed runoff before July and also matches the observed streamflow peaks and low flows

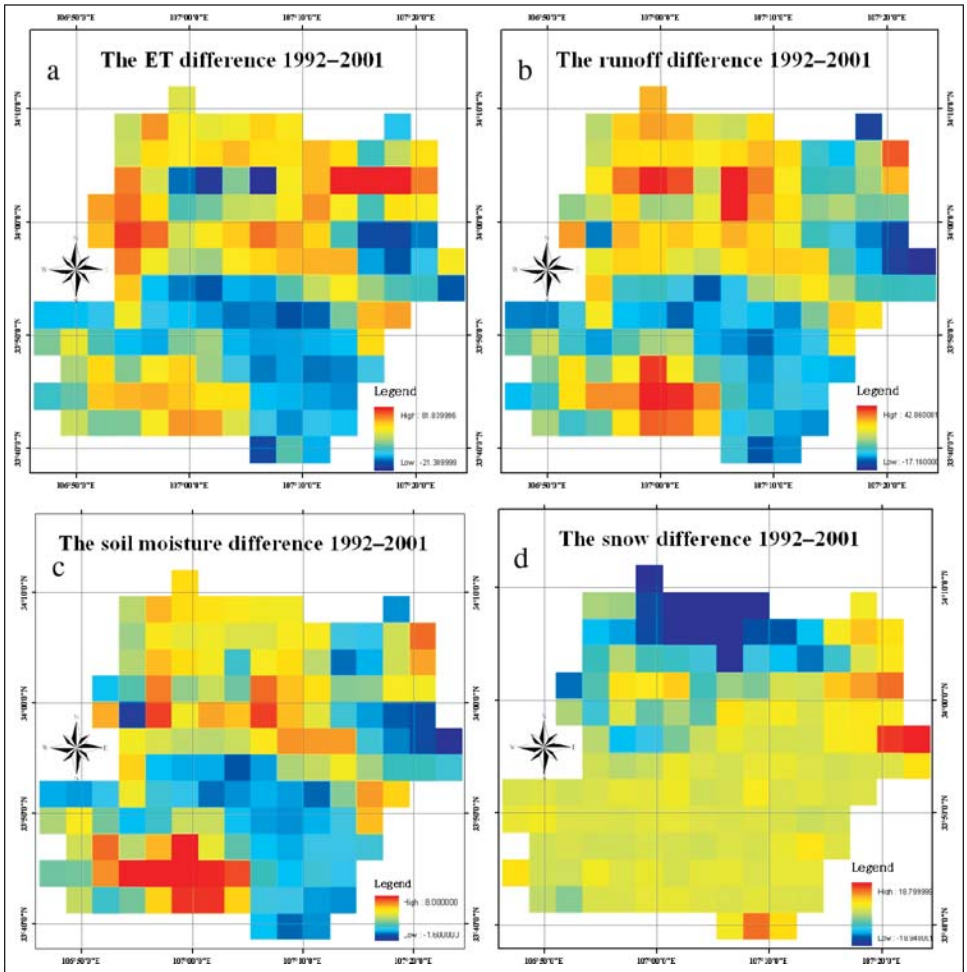

Figure 9. Spatial distribution differences between the VIC-3L model simulations using MODIS vegetation data and those using REDC vegetation data: (a) mean annual evapotranspiration, (b) mean annual runoff, (c) mean annual soil moisture in the top 10 cm layer, and (d) mean annual snow sublimation.

in July and August. The significant underestimations of the observed peaks by the VIC-3L model in May, June, July, and October are all improved in 1999. On the other hand, the VIC-3L model overestimates smaller peaks in April and September. In 2001, the use of MODIS vegetation data results in a remarkable improvement in the peak flow simulation by the VIC-3L model in September, while there is little change in runoff simulations for the other months.

The results show that the MODIS vegetation data, such as land cover and LAI, are helpful in improving hydrologic simulations. This is because the LAI and land cover information derived from MODIS data reflects more accurate vegetation classifications and the seasonal variations. The REDC land cover information is outdated and too general, with only six vegetation types identified. In fact, there are usually mixed forests in the Baohe basin. The large deciduous broadleaf forest identified by the REDC resulted in an increase in evapotranspiration and a decrease in runoff, which leads to a decrease in streamflow simulation. This is probably why the peak flow simulations with the REDC are considerably lower than the observed peak flows, whereas the simulated results with the MODIS data are closer to the observations.

Conclusion

This study shows that the stepwise interpolation approach (SIA) method is effective in interpolating the climate variables to obtain reasonable spatial distributions of the atmospheric forcings needed in the VIC-3L model. The VIC-3L model can reasonably simulate water fluxes such as evapotranspiration, runoff, soil moisture, and snow sublimation for the Baohe River basin if reasonable vegetation information is available. The much more reasonable spatial distributions and magnitude of vegetation classification and LAI of the MODIS data source than those from the REDC data source clearly demonstrate that vegetation information significantly affects the spatial distribution of evapotranspiration, and thus the spatial distributions of runoff, soil moisture, and other water fluxes, and also their magnitudes. This study shows the important role that remote sensing information (e.g., MODIS data) can play in

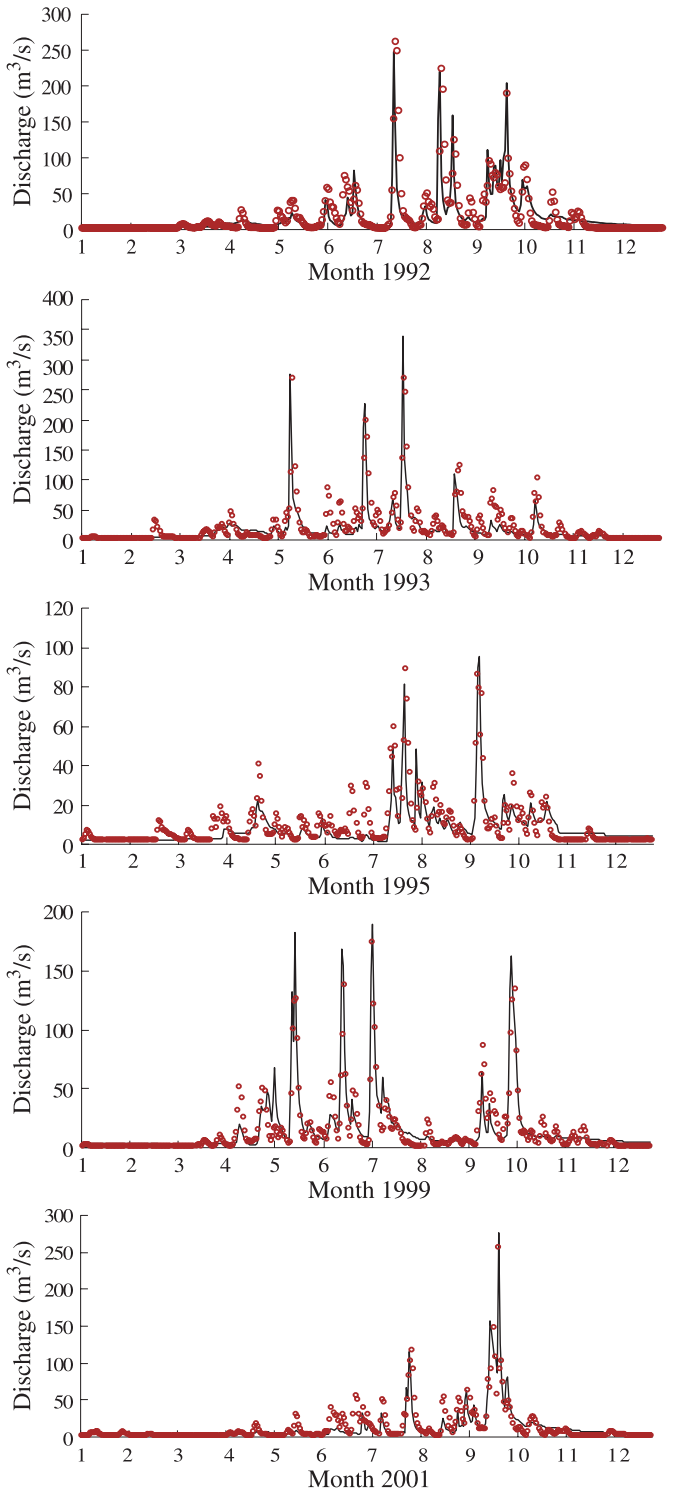

Figure 10. Comparison of the VIC-3L model simulated daily flow (open circles) based on the MODIS vegetation information with the observed streamflow (solid lines) at Jiangkou hydrological station at the outlet of the Baohe River basin for 5 years during the period 1992–2001.

improving land surface model simulations. Since this is the first study of applying VIC-3L to the Yangtze River basin in China with a high level of spatial resolution, the promising results obtained here are quite encouraging for future applications of the VIC-3L model to the entire basin.

Acknowledgements

Funding for this work was provided by the Ministry of Science and Technology and the National Natural Science Foundation of China (project numbers 2001CB309404, 40128001/D05, and 49375248).

References

Ayenew, T. 2003. Evapotranspiration estimation using thematic mapper spectral satellite data in the Ethiopian rift and adjacent highlands. *Journal of Hydrology*, Vol. 279, pp. 83–93.

Basist, A., Bell, G.D., and Meentenmeyer, V. 1994. Statistical relationships between topography and precipitation patterns. *Journal of Climate*, Vol. 7, No. 9, pp. 1305–1315.

Bastiaanssen, W.G.M., Menenti, R.A., and Holtslag, F. 1998. The surface energy balance algorithm for land (SEBAL). Part 1. Formulation. *Hydrobiologia*, Vol. 213, pp. 198–298.

Bowling, L.C., Lettenmaier, D.P., Nijssen, B., et al. 2003. Simulation of high latitude hydrological processes in the Torne-Kalix basin: PILPS Phase 2(e) 1: Experiment description and summary intercomparisons. *Global and Planetary Change*, Vol. 38, Nos. 1–2, pp. 1–30.

Chen, T., Henderson-Sellers, A., Milly, P.C.D., et al. 1997. Cabauw experimental results from the project for intercomparison of land-surface parameterization schemes (PILPS). *Journal of Climate*, Vol. 10, No. 6, pp. 1194–1215.

Cherkauer, K.A., and Lettenmaier, D.P. 1999. Hydrologic effects of frozen soils in the upper Mississippi River basin. *Journal of Geophysical Research*, Vol. 104, No. D16, pp. 19 599 – 19 610.

Engman, E.T. 1996. Remote sensing applications to hydrology: future impact. *Hydrological Sciences*, Vol. 41, pp. 637–647.

Famiglietti, J.S., Devereaux, J.A., Laymon, C.A., et al. 1999. Ground-based investigation of soil moisture variability within remote sensing footprints during the Southern Great Plains 1997 (SGP97) Hydrology Experiment. *Water Resources Research*, Vol. 35, No. 6, pp. 1839–1851.

Francini, M., and Pacciani, M. 1991. Comparative analysis of several conceptual rainfall–runoff models. *Journal of Hydrology*, Vol. 122, pp. 161–219.

Gillies, R.R., Carlson, T.N., Cui, J., et al. 1997. A verification of the triangle method for obtaining surface soil water content and energy fluxes from remote measurements of the normalized difference vegetation index (NDVI) and surface radiant temperature. *International Journal of Remote Sensing*, Vol. 18, No. 15, pp. 3145–3166.

Goodale, C.L., Alber, J.D., and Ollinger, S.V. 1998. Mapping monthly precipitation, temperature and solar radiation for Ireland with polynomial regression and digital elevation model. *Climate Research*, Vol. 10, pp. 35–49.

Goovaerts, P. 2000. Geostatistical approaches for incorporating elevation into the spatial interpolation of rainfall. *Journal of Hydrology*, Vol. 228, Nos. 1–2, pp. 113–129.

Hamlet, A.F., and Lettenmaier, D.P. 1999a. Effects of climate change on hydrology and water resources in the Columbia River basin. *Journal of the American Water Resources Association*, Vol. 35, No. 6, pp. 1597–1623.

Hamlet, A.F., and Lettenmaier, D.P. 1999b. Columbia River streamflow forecasting based on ENSO and PDO climate signals. *Journal of Water Resources Planning and Management, ASCE*, Vol. 125, No. 6, pp. 333–341.

Hupet, F., and Vanclooster, M. 2002. Intraseasonal dynamics of soil moisture variability within a small agricultural maize cropped field. *Journal of Hydrology*, Vol. 261, pp. 86–101.

Jiang, L., and Islam, S. 2001. Estimation of surface evaporation map over southern Great Plains using remote sensing data. *Water Resources Research*, Vol. 37, No. 2, pp. 329–340.

Kim, G., and Barros, A.P. 2002. Space–time characterization of soil moisture from passive microwave remotely sensed imagery and ancillary data. *Remote Sensing of Environment*, Vol. 81, pp. 393–403.

Knyazikhin, Y., Martonchik, J.V., Myneni, R.B., et al. 1998a. Synergistic algorithm for estimating vegetation canopy leaf area index and fraction of absorbed photosynthetically active radiation from MODIS and MISR data. *Journal of Geophysical Research*, Vol. 103, No. D24, pp. 32 257 – 32 276.

Knyazikhin, Y., Martonchik, J.V., Diner, D.J., et al. 1998b. Estimation of vegetation canopy leaf area index and fraction of absorbed photosynthetically active radiation from atmosphere corrected MISR data. *Journal of Geophysical Research*, Vol. 103, No. D24, pp. 32 239 – 32 256.

Kurtzman, D., and Kadmon, R. 1999. Mapping of temperature variables in Israel: a comparison of different interpolation methods. *Climate Research*, Vol. 13, pp. 33–43.

Leung, L.R., Hamlet, A.F., Lettenmaier, D.P., and Kumar, A. 1999. Simulations of the ENSO hydroclimate signals in the Pacific Northwest Columbia River basin. *Bulletin of the American Meteorological Society*, Vol. 80, No. 11, pp. 2313–2329.

Liang, X., and Xie, Z. 2001. A new surface runoff parameterization with subgrid-scale soil heterogeneity for land surface models. *Advances in Water Resources*, Vol. 24, Nos. 9–10, pp. 1173–1193.

Liang, X., Lettenmaier, D.P., Wood, E.F., and Burges, S.J. 1994. A simple hydrologically based model of land surface water and energy fluxes for general circulation models. *Journal of Geophysical Research*, Vol. 99, No. D7, pp. 14 415 – 14 428.

Liang, X., Lettenmaier, D.P., and Wood, E.F. 1996a. A one-dimensional statistical dynamic representation of subgrid spatial variability of precipitation in the two-layer variable infiltration capacity model. *Journal of Geophysical Research*, Vol. 101, No. D16, pp. 21 403 – 21 422.

Liang, X., Wood, E.F., and Lettenmaier, D.P. 1996b. Surface soil moisture parameterization of the VIC-2L model: evaluation and modifications. *Global and Planetary Change*, Vol. 13, No. 1, pp. 195–206.

Liang, X., Wood, E.F., Lettenmaier, D.P., et al. 1998. The project for intercomparison of land-surface parameterization schemes (PILPS) phase-2c Red-Arkansas river basin experiment: 2. Spatial and temporal analysis of energy fluxes. *Global and Planetary Change*, Vol. 19, No. 1–4, pp. 137–159.

Liang, X., Wood, E.F., and Lettenmaier, D.P. 1999. Modeling ground heat flux in land surface parameterization schemes. *Journal of Geophysical Research*, Vol. 104, No. D8, pp. 9581–9600.

Liang, X., Xie, Z., and Huang, M. 2003. A new parameterization for surface and groundwater interactions and its impact on water budgets with the variable infiltration capacity (VIC) land surface model. *Journal of Geophysical Research*, Vol. 108, No. D16, Art. No. 8613.

Lohmann, D., and Nolte-Holube, R. 1996. A large scale horizontal routing model to be coupled to land surface parameterization schemes. *Tellus*, Vol. 48A, pp. 708–721.

Lohmann, D., Lettenmaier, D.P., Liang, X., et al. 1998. The project for intercomparison of land-surface parameterization schemes (PILPS) phase 2(c) Red–Arkansas River basin experiment: 3. Spatial and temporal analysis of water fluxes. *Global and Planetary Change*, Vol. 19, No. 1, pp. 161–179.

Marquínez, J., Lastra, J., and Garcia, P. 2003. Estimation models for precipitation in mountainous regions: the use of GIS and multivariate analysis. *Journal of Hydrology*, Vol. 270, pp. 1–11.

Martíinez-Cob, A. 1996. Multivariate geostatistical analysis of evapotranspiration and precipitation in mountainous terrain. *Journal of Hydrology*, Vol. 174, Nos. 1–2, pp. 19–35.

Mohanty, B.P., and Skaggs, T.H. 2001. Spatio-temporal evolution and time-stable characteristics of soil moisture within remote sensing footprints with varying soil, slope, and vegetation. *Advances in Water Resources*, Vol. 24, pp. 1051–1067.

Nijssen, B., Lettenmaier, D.P., Liang, X., et al. 1997. Streamflow simulation for continental-scale river basins. *Water Resources Research*, Vol. 33, No. 4, pp. 711–724.

Nijssen, B., O'Donnell, G.M., Hamlet, A.F., and Lettenmaier, D.P. 2001a. Hydrologic sensitivity of global rivers to climate change. *Climatic Change*, Vol. 50, Nos. 1–2, pp. 143–175.

Nijssen, B., O'Donnell, G.M., Lettenmaier, D.P., et al. 2001b. Predicting the discharge of global rivers. *Journal of Climate*, Vol. 14, No. 15, pp. 3307–3323.

Nijssen, B., Bowling, L.C., Lettenmaier, D.P., et al. 2003. Simulation of high latitude hydrological processes in the Torne–Kalix basin: PILPS Phase 2(e) 2: Comparison of model results with observations. *Global and Planetary Change*, Vol. 38, Nos. 1–2, pp. 31–53.

Ninyerola, M., Pons, X., and Roure, J.M. 2000. A methodological approach of climatological modeling of air temperature and precipitation through GIS techniques. *International Journal of Climatology*, Vol. 20, No. 14, pp. 1823–1841.

Oldak, A., Pachepsky, Y., Jackson, T.J., and Rawls, W.J. 2002. Statistical properties of soil moisture images revisited. *Journal of Hydrology*, Vol. 255, pp. 12–24.

Olivera, M.A., and Webster, R. 1990. Kriging: a method of interpolation for geographical information systems. *International Journal of Geographic Information Systems*, Vol. 4, No. 3, pp. 313–332.

Parada, L.M., Fram, J.P., and Liang, X. 2003. Multi-resolution calibration methodology for hydrologic models: Applications to a sub-humid catchment. In *Advances in calibration of watershed models*. Edited by Q. Duan, H. Gupta, S. Sorooshian, A. Rousseau, and R. Turcotte. Water Science and Application 6, American Geophysical Union, Washington, D.C. pp. 197–211.

Prudhomme, C., and Reed, D.W. 1999. Mapping extreme rainfall in a mountainous region using geostatistical techniques: a case study in Scotland. *International Journal of Climatology*, Vol. 19, No. 12, pp. 1337–1356.

Reed, S.M. 2003. Deriving flow directions for coarse-resolution (1–4 km) gridded hydrologic modeling. *Water Resources Research*, Vol. 39, No. 9, Art. No. 1238.

Ritchie, J.C., and Rango, A. 1996. Remote sensing applications to hydrology: introduction. *Hydrological Sciences*, Vol. 41, pp. 429–431.

Todini, E. 1996. The ARNO rainfall–runoff model. *Journal of Hydrology*, Vol. 175, pp. 339–382.

Weisse, A.K., and Bois, P. 2001. Topographic effects on statistical characteristics of heavy rainfall and mapping in the French Alps. *Journal of Applied Meteorology*, Vol. 40, No. 4, pp. 720–740.

Wood, F., Lettenmaier, D.P., Liang, X., et al. 1997. Hydrological modeling of continental-scale basins. *Annual Review of Earth and Planetary Sciences*, Vol. 25, pp. 279–300.

Wood, F., Lettenmaier, D.P., Liang, X., et al. 1998. The project for intercomparison of land-surface parameterization schemes (PILPS) phase-2c Red–Arkansas River basin experiment: 1. Experiment description and summary intercomparisons. *Global and Planetary Change*, Vol. 19, No. 1, pp. 115–135.

Wotling, G., Bouvier, Ch., Danloux, J., and Fritsch, J.M. 2000. Regionalization of extreme precipitation distribution using the principal components of the topographical environment. *Journal of Hydrology*, Vol. 233, pp. 86–101.

Zhou, S. 1993a. The analysis method of sunshine percentage for high resolution. *Scientia Meteorologica Sinica*, Vol. 16, No. 3, pp. 16–28.

Zhou, S. 1993b. The analysis method of global radiation in mountain areas for high resolution. *Journal of Low-Latitude Plateau Weather*, Vol. 6, No. 1, pp. 33–45.

Zhou, S. 1995. The analysis method of precipitation in mountain area for high resolution. In *The utilization and development of climate resource in mountain area*. China Meteorological Press, Beijing, China. pp. 74–86.